Available online at www.sciencedirect.com
ScienceDirect
Journal of Magnetic Resonance 185 (2007) 42–49
JMR Journal of Magnetic Resonance
www.elsevier.com/locate/jmr

The effects of SNR on ADC measurements in diffusion-weighted hyperpolarized He-3 MRI ☆

Rafael L. O'Halloran [a], James H. Holmes [a], Talissa A. Altes [c,d], Michael Salerno [e], Sean B. Fain [a,b,*]

[a] *Department of Medical Physics, University of Wisconsin, Madison, WI, USA*
[b] *Department of Radiology, University of Wisconsin, Madison, WI, USA*
[c] *Department of Radiology, Children's Hospital of Philadelphia, Philadelphia, PA, USA*
[d] *University of Virginia, Charlottesville, VA, USA*
[e] *Duke University Medical Center, Durham, NC, USA*

Received 25 July 2006; revised 21 September 2006
Available online 5 December 2006

Abstract

The theoretical dependence of the mean and standard deviation of ADC values on signal-to-noise ratio (SNR) was derived and compared to measured values in porous phantoms and the lungs of human subjects using diffusion-weighted hyperpolarized helium-3 MRI. For SNR values below 15, mean ADC values were highly SNR-dependent due to a combination of noise and choice of noise thresholding. Above SNR values of 15 and for mean ADC values within ranges relevant for evaluating lung disease (<0.6 cm^2/s), the mean ADC was largely independent of SNR. The standard deviation, by contrast, was highly dependent on SNR over a much larger range, but this dependence was well predicted by theory, suggesting the histogram of ADC values might be corrected for these stochastic processes to more accurately evaluate disease using restricted diffusion measures in the lungs.

Keywords: Diffusion; Lung; ADC; SNR

1. Introduction

In diffusion-weighted MRI, a measurement of the apparent diffusion coefficient (ADC) can be obtained by doing a pulsed gradient spin echo experiment and assuming a mono-exponential model [1]. ADC can depend on spatial and time-dependent factors due to tissue structures that restrict diffusion regionally [2]. The ADC for hyperpolarized (HP) helium-3 MRI in the lung has shown the potential to be a useful and reproducible [3,4] measurement in the diagnosis of obstructive lung disorders such as emphysema because it can be sensitive to changes in alveolar structures [5]. Specific to lung, ADC measures allow the detection of emphysematous tissue changes before the onset of other observable symptoms [6,7]. The current diagnostic standard is spirometry, which has been shown to correlate with ADC measurements [8] and high resolution CT [9]. The advantage of ADC over spirometry is the ability to do quantitative regional analysis [10]. Emphysema is a heterogeneous disease [9,11] and ADC maps can provide a means to evaluate regional severity for guiding surgical interventions [12]. Moreover, preliminary results suggest that ADC metrics may be more sensitive than CT densitometry [11,13,14].

However, ADC measures of the gas diffusion in the lung are known to be biased under conditions of low signal-to-noise ratio (SNR) [3,4]. Insufficient SNR can lead to spuriously low mean ADC values and high standard deviation (SD). It would be advantageous to minimize this depen-

☆ *Statement of funding:* Award to SBF from the Sandler Program for Asthma Research.
* Corresponding author. Fax: +1 608 265 9840.
E-mail address: sfain@wisc.edu (S.B. Fain).

1090-7807/$ - see front matter © 2007 Published by Elsevier Inc.
doi:10.1016/j.jmr.2006.11.006

dence by appropriate thresholding or to know a priori the minimum SNR required to obtain an accurate measurement of the mean ADC. Similarly it may be of value to retrospectively isolate stochastic variation from true structural variation to capture SD measurements that accurately reflect deterministic structural variations, rather than stochastic processes.

One approach to reduce the SNR-dependent bias in ADC measures is to apply a fixed noise threshold to both the diffusion-weighted and -unweighted images [15]. In the thresholding technique of Salerno et al. [8,15], approximately 90% of the pixels containing signal are kept at the 2.5σ threshold. Therefore, the threshold is set to 2.5σ, where σ is the standard deviation of the statistically independent and presumably equivalent noise levels in the in-phase and quadrature channels. Because the measured noise is therefore the magnitude of an originally complex noise process, the measured noise background, σ_M, has been shown to be related to σ by $\sigma_M^2 = (2-\pi/2)\sigma^2$ [16,17]. However, Morbach et al. [4] used two different noise thresholds, a milder threshold in the diffusion-weighted relative to the unweighted image in recognition that voxels with high ADC values might still be valid measurements that fall near σ_M.

The purpose of the present work is two-fold. First, to rigorously present the dependence of ADC measures on SNR for the commonly used mono-exponential decay model, and, second, determine an appropriate minimum SNR requirement for the accurate calculation of mean ADC values from images derived from diffusion-weighted HP gas data in the lungs.

2. Theory

2.1. ADC vs. SNR

For a mono-exponential model [11], an ADC map can be calculated on a voxel-by-voxel basis from two images, one diffusion-weighted with signal S_1 and one unweighted with signal S_0. For HP diffusion-weighted MRI, the mono-exponential model is routinely applied because two image sets can usually be obtained in a breath-hold. Using these methods, the ADC map is computed for each voxel according to,

$$\mathrm{ADC} = \frac{1}{b}\cdot \ln\left(\frac{S_0}{S_1}\right), \tag{1}$$

where b is a parameter that depends on the timing and amplitude of the diffusion weighting gradients. It is reasonable to assume the same noise level, σ, in the weighted and unweighted images since the noise processes are dominated by factors unrelated to the diffusion weighting. It is further assumed that the noise in these images is uncorrelated. Given these assumptions, we can redefine Eq. (1) in terms of signal-value-to-noise ratio (SVNR) in each voxel of the weighted and unweighted images, SVNR_1 and SVNR_0 respectively,

$$\mathrm{ADC} = \frac{1}{b}\cdot \ln\left(\frac{\mathrm{SVNR}_0}{\mathrm{SVNR}_1}\right). \tag{2}$$

The SVNR is related to the estimated SNR by taking the average SVNR for a given range or region in the image:

$$\mathrm{SNR} = \frac{1}{N}\sum_i^N \mathrm{SVNR}_i = \frac{1}{N\sigma}\sum_i^N S_{0_i} = \frac{\bar{S}_0}{\sigma}, \tag{3}$$

where N is the total number of pixels in the range. The SVNR measure is a noise-normalized measure that is useful in describing the effects of SNR on ADC measures. The convention used in this paper is that the SVNR term refers to the unweighted image, SVNR_0, unless otherwise denoted.

2.2. Stochastic analysis

An analytical expression for the ADC as a function of SVNR is obtained by recognizing that the SVNR_0 and SVNR_1 are Rician distributed random variables [16,18]. A Rician distributed random variable is formed by performing a magnitude operation on two independent Gaussian distributed random variables. In MRI, the noise in a magnitude image, therefore, is Rician when the constituent noise in the real and imaginary channels is Gaussian [17]. To determine the probability distribution function (PDF) for the measured ADC we rewrite Eq. (2) and define two random variables RV_1 and RV_2,

$$\mathrm{ADC} = \frac{\ln \mathrm{SVNR}_0}{b} - \frac{\ln \mathrm{SVNR}_1}{b} \equiv \mathrm{RV}_1 + \mathrm{RV}_2, \tag{4a}$$

$$\mathrm{RV}_1 \equiv \frac{\ln \mathrm{SVNR}_0}{b}, \tag{4b}$$

$$\mathrm{RV}_2 \equiv \frac{-\ln \mathrm{SVNR}_1}{b}. \tag{4c}$$

Since the PDFs of SVNR_0 and SVNR_1 are known we use the functional dependence of RV_1 and RV_2 on SVNR_0 and SVNR_1 given by Eqs. (4b and c) to determine the PDFs of RV_1 and RV_2. Using the theory of random variables the functional dependence of the ADC is therefore:

$$P_{\mathrm{ADC}}(\mathrm{ADC}) = P_{\mathrm{RV}_1}(\mathrm{RV}_1) \ * \ P_{\mathrm{RV}_2}(\mathrm{RV}_2), \tag{5}$$

where '*' denotes the convolution operator. Here the PDF is denoted by 'P' with a subscript to identify the random variable. A more detailed derivation is given in Appendix A.

2.3. Standard deviation of ADC vs. SNR

Moreover, the theoretical dependence of the standard deviation of the ADC, σ_{ADC}, is shown to be,

$$\sigma_{\mathrm{ADC}} = \frac{1}{b}\cdot\frac{1}{\mathrm{SVNR}_0}\cdot\sqrt{1+e^{2\cdot b\cdot \mathrm{ADC}}}, \tag{6}$$

in Appendix Eqs. (A9)–(A12), where again the noise is assumed to be uncorrelated in the weighted and unweighted

images. Experimental evidence for the validity of Eq. (6) will be provided in Section 4.

3. Methods

3.1. Monte carlo simulation

A 128-element vector, A_i, was assigned 128 equally spaced initial signal values from 10 to 750 and used to create corresponding vectors, B_i, representing the diffusion-weighted signal, related by,

$$B_i = A_i \cdot \exp(-b \cdot \mathrm{ADC}). \tag{7}$$

A fixed b-value of 1.6 s/cm^2, and nominal values of ADC ranging from 0.2 to 1.0 cm^2/s were used. Vectors A_i' and B_i' were formed by adding zero mean Gaussian noise ($\sigma = 10$) to A_i and B_i respectively. ADC values were then calculated by rearranging Eq. (7) and using the primed vectors according to,

$$\mathrm{ADC} = \frac{1}{b} \cdot \ln\left|\frac{A_i'}{B_i'}\right|. \tag{8}$$

This process was repeated 400 times to obtain sufficient statistics. The resulting data points were binned according to SVNR and averaged, resulting in a mean ADC vs. SVNR curve. Comparisons were done using thresholding at 0, 2.5, 5 and 7.5 times σ.

3.2. Phantom construction

The above theory was validated in phantom studies. Two phantoms were constructed from 5 cm inner diameter PVC pipe sealed at each end with end-caps. One end-cap on each phantom had a hole fitted with 1/8″-inner-diameter Tygon tube (US Plastic Corp., Lima, OH, USA) to allow evacuation and filling. One phantom contained porous polyurethane foam (density = 48 mg/cc) resulting in a 180 cc net volume. Pore size in the foam was estimated by measuring the diameter of 20 pores from a digital scanner image. The average pore size was 270 ± 60 μm. The free diffusion phantom was vacant with a volume of 110 cc.

3.3. HP gas production

HP ^{3}He gas was polarized using spin-exchange optical pumping [19] to polarize ^{3}He to 30–40%. The phantom and Tedlar gas sample bags (Jensen Inert Inc., Coral Springs, FL, USA) were evacuated and purged with nitrogen several times before filling with ^{3}He to 1 atm. For phantom studies the ^{3}He was drawn from the polarizing unit directly into the phantom via a 1/8″-diameter Tygon tube. For human studies a 'dose' of HP ^{3}He was prepared by drawing ^{3}He into the gas sample bag from the polarizing unit and mixing with pure N_2 until the concentration of hyperpolarized nuclei was 4.5 mM at a total volume of 15% of the subject's total lung volume.

3.4. Magnetic resonance imaging

All experiments were carried out with a 2D axial diffusion weighted scan with a b-value of 1.6 s/cm^2 on a 1.5 T MR scanner with broadband capabilities (Signa LX, GE Healthcare, Milwaukee, WI). As recent work has shown, the choice of b-value can be optimized depending on the expected SNR and ADC in the experiment [20]. Here, the particular b-value was chosen to preserve SNR in the diffusion-weighted image over the range of ADC values expected in healthy and diseased human parenchyma (0.1–0.5 cm^2/s). To simplify the present investigation and to address the method most commonly used in the literature we assume a mono-exponential model. The diffusion encoding gradient was perpendicular to the slice. A chest coil (IGC-InVivo Research, Milwaukee, WI) tuned to the ^{3}He resonant frequency was used to transmit and receive. Phantom imaging was carried out using a fast-GRE sequence, with a 31.25 kHz readout bandwidth, 64×64 image matrix, 1 slice, ~4 cm slice thickness, TR/TE of 7 ms/3.6 ms and flip angle of ≈7°. A large axial slice was used because the phantoms were symmetric along the B_0 field. A series of images was obtained without changing the gas by allowing RF saturation to further degrade the SNR at each subsequent image. Experimental results were obtained in 19 human subjects (Mean age = 45.6 ± 4 yrs, range = 23–73 yrs, 10 males, 9 females). For the human studies imaging parameters included 31.25 kHz readout bandwidth, 128×80 image matrix, 10 slices, 1.5 cm slice thickness, TR/TE of 8.4 ms/4.5 ms and flip angle of ≈7°. Flip angles were calibrated using a pulse-acquire sequence. The peak of the Fourier transform of the free induction decay signals obtained from the phantoms were fit to the model:

$$S(\alpha, n) = \sin\alpha \cos\alpha^{n-1}, \tag{9}$$

where n is an index of the number of excitation rf-pulses applied and flip angle, α.

3.5. Data analysis

The true noise standard deviation, σ, was determined by measuring the standard deviation in an ROI in the noise field, σ_M, and correcting it via $\sigma_M^2 = (2 - \pi/2)\sigma^2$. The SVNR was then calculated by dividing the signal in each pixel by σ as for the simulations. ADC values were calculated using Eq. (1) and their mean and standard deviation were obtained by binning the data according to the measured SVNR in the unweighted image and calculating the mean and standard deviation within each bin. The bin width used was ±8.5 SVNR values for phantoms and ±1.75 SVNR values for human subjects, providing 20 bins over the available range of SNR values. A routine for performing these calculations for the ADC values was implemented using MATLAB (MathWorks, Natick, MA). All image processing and data analysis was performed on the magnitude images.

4. Results

4.1. Analytical results

In Fig. 1, the functional dependence of the mean ADC values on SNR are depicted for true mean ADC values of 0.2 and 0.8 cm^2/s—typical values expected in normal human volunteers in lung parenchyma and the airways respectively. From the numerical evaluation of Eq. (5), an error of less than 0.2% in the mean ADC is predicted for ADC values less than 0.6 cm^2/s at an SNR above 15 (Table 1). Fig. 1 shows graphically the functional dependence of the probability distribution of the ADC for SNRs of 6 and 15 in the unweighted image. At a given expected ADC value the distribution becomes increasingly dispersed and skewed towards lower values as the intrinsic SNR of the experiment drops. For, lower ADC values, i.e. increased level of restriction in our model, the probability distribution is less dependent on SNR because the signal loss due to diffusion is reduced by the higher restriction in the airspaces. Smaller signal reduction results in less data below the noise level.

4.2. Simulations

For the results of the Monte Carlo simulation, the ensemble average of all voxels with similar SVNR is an estimate of the SNR for voxels in the given signal range, Eq. (3). Therefore, given sufficient number of samples at each SVNR, the mean ADC can be estimated directly from the ADC vs. SVNR plot (Fig. 2) and compared to the theoretical dependences predicted in Fig. 1. In Fig. 2A the ADC vs. SVNR dependence (yellow line) for the fixed threshold value of 2.5σ is shown superimposed on all SVNR values. The thresholding process affects ADC at lower SVNR by rejecting the blue data points that correspond to values in the upper tail of the ADC probability distributions shown in Fig. 1. The green lines indicate the threshold separating the voxels retained (red) for the voxels rejected (blue).

The stochastic dependence of the standard deviation of the ADC is shown in Fig. 2B. The theoretical values given by Eq. (6) are represented as green error bars and appear adjacent to the corresponding measured errors shown in yellow. The green error bars are offset to the right to aid visualization. Mean values of each bin are indicated by the red points connected by the red line. Because the simulation is governed entirely by stochastic processes the results agree quite well, whereas in human subjects the actual standard deviation will exceed the predicted value due to physiological and structural sources of variation.

The measured mean ADC plotted vs. SVNR are shown in Fig. 3A–D for different threshold values and ADC val-

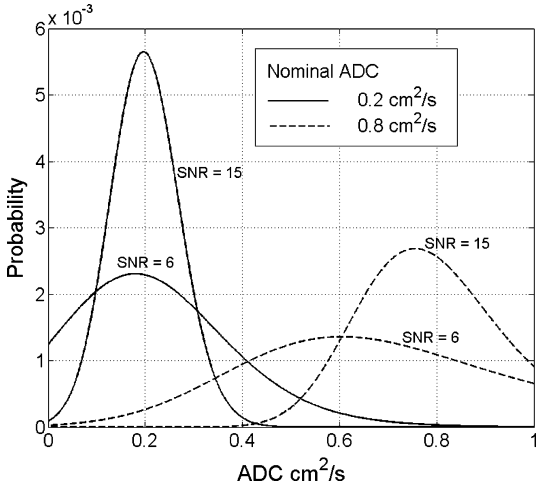

Fig. 1. Probability distribution of the ADC values for diffusion coefficients of 0.2 cm^2/s and 0.8 cm^2/s and at SNR values of 6 and 15 in the unweighted image. The decrease in mean ADC and the increase in dispersion with decreased SNR is qualitatively apparent.

Table 1
Percent error in Mean ADC for specific SNR values

Mean ADC cm^2/s	SNR_0			
	5 (%)	10 (%)	15 (%)	20 (%)
0.2	0.7	0.05	0.016	
0.4	1.7	0.12	0.092	0.075
0.6	4.6	0.38	0.12	0.025
0.8	10	1.4	0.27	0.13

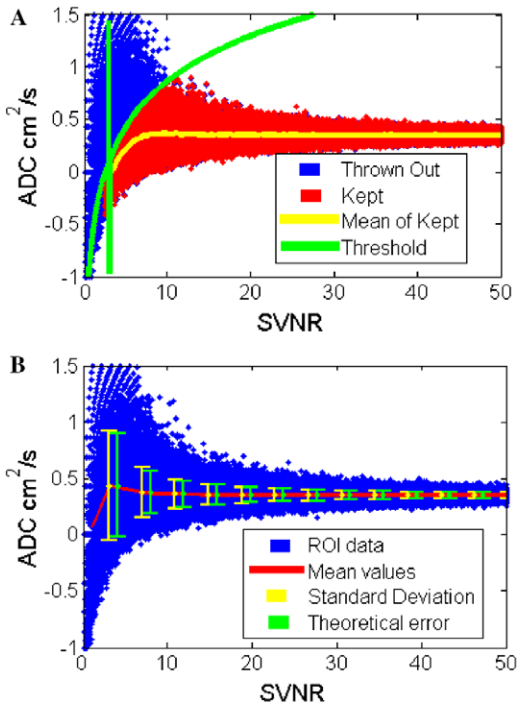

Fig. 2. ADC simulation data shown in (A) with Eq. (2) plotted in green for a threshold value of 2.5σ. Points in blue are rejected, leaving points in red for ROI based calculations. The running mean of the retained data points is plotted in yellow. The standard deviation of the unthresholded distribution is shown (B) with yellow bars compared to the theoretical standard deviation shown in green bars. At higher SVNR values the measured values overlap the theoretical values as expected.

ues. When no threshold is applied (Fig. 3A), there is an initial overshoot resulting from spuriously high ADC values calculated from very low SNR_1 voxels in the weighted image. While thresholding eliminates these spurious values (Fig. 3B–D), the SNR dependence due to the relationship in Eq. (2) leads to an underestimation of the mean ADC, even for a relatively mild noise threshold of 2.5 times σ. Note that underestimation is more pronounced for higher values of ADC and for higher noise threshold values.

4.3. Experiments

A typical ADC image and histogram for a 60 year old male with a 35 pack year smoking history is shown in Fig. 4. A ventilation defect (white arrow) on the left side of the image is clearly seen. Fig. 5 shows a typical SNR dependence of the ADC for human lungs, in this specific case a 60 year old male with a 40 pack year smoking history. The mean ADC values (solid black line) for SNR bins at a threshold of 2.5σ (dotted line) are shown. Note that the mean ADC drops rapidly for $SNR_0 < 10$, similar to that observed for the simulation studies. This rapid falloff in the mean was observed to occur at an average $SNR_0 = 10 \pm 1$ for the 19 human subjects and did not vary significantly with disease.

Fig. 6A–C shows the dependence of the mean ADC and σ_{ADC} on SNR_0 in the free diffusion phantom, the foam phantom and human lung. The dependence of σ_{ADC} on SNR_0 in the free diffusion phantom (Fig. 6A) agrees quite well with the stochastic dependence predicted by Eq. (6). However in the foam phantom (Fig. 6B) and human data (Fig. 6C), SD_{ADC} is consistently larger than the value predicted by Eq. (6). This suggests that the source of the additional variance in the foam and human lung data is likely due to physical variation in the underlying microstructure.

5. Discussion

Theoretical and experimental studies demonstrate the dependence of ADC measures on SNR for HP DW-MRI in the lung. The observed ADC vs. SNR behavior has been shown to be a direct result of thresholding and noise propagation due to the form of Eq. (1) using simulation and phantom studies. At a given SNR, the ADC values form a distribution about the mean but when the SNR is insufficient, the thresholding process significantly truncates the upper tail of this distribution, driving the mean below its true value. At sufficiently high SNR the ADC is independent of SNR. According to theory and experiment, the

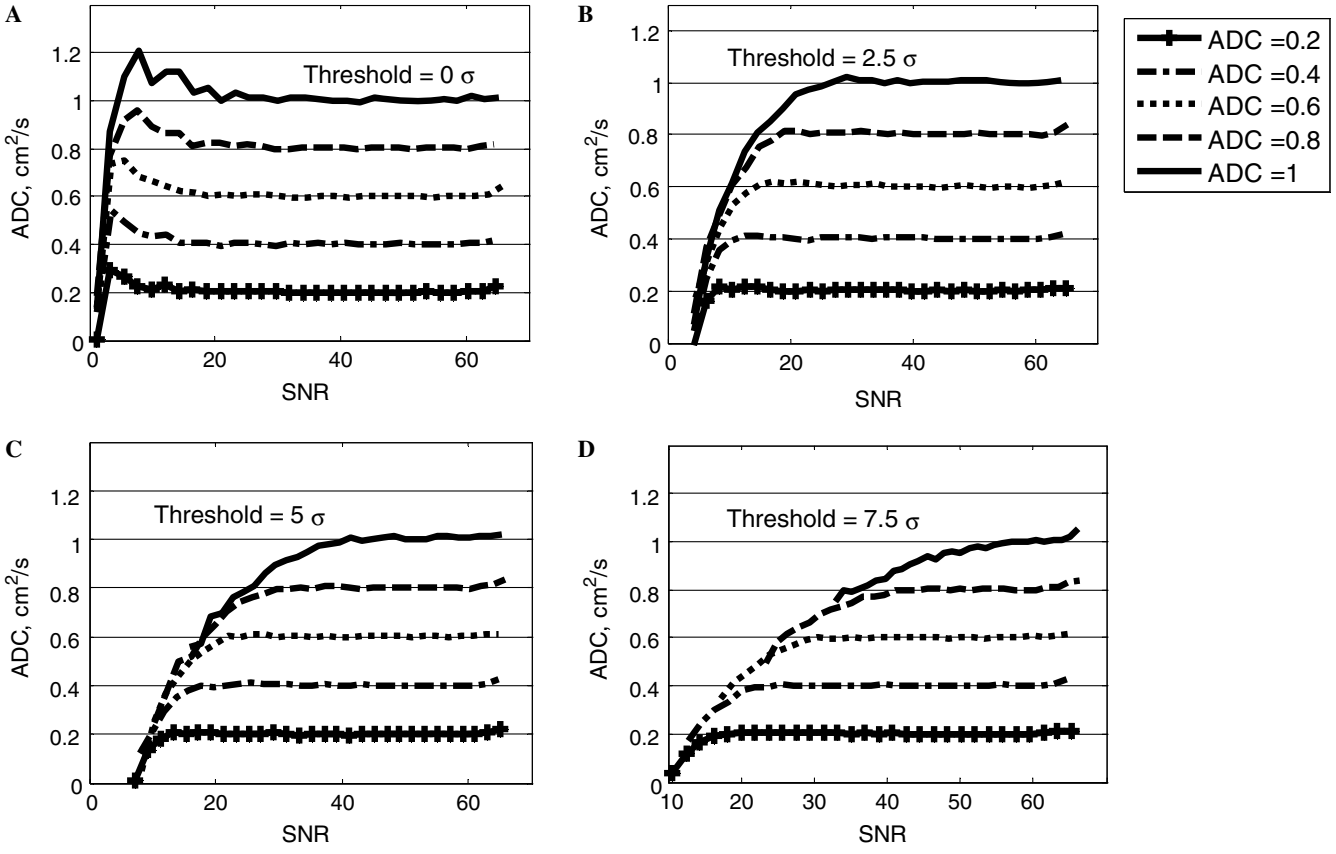

Fig. 3. ADC vs. SNR behavior for simulation experiments (A–D). Increasing threshold values are as indicated with the noise held constant. Note that as the threshold increases, the mean ADC is increasingly biased towards lower values.

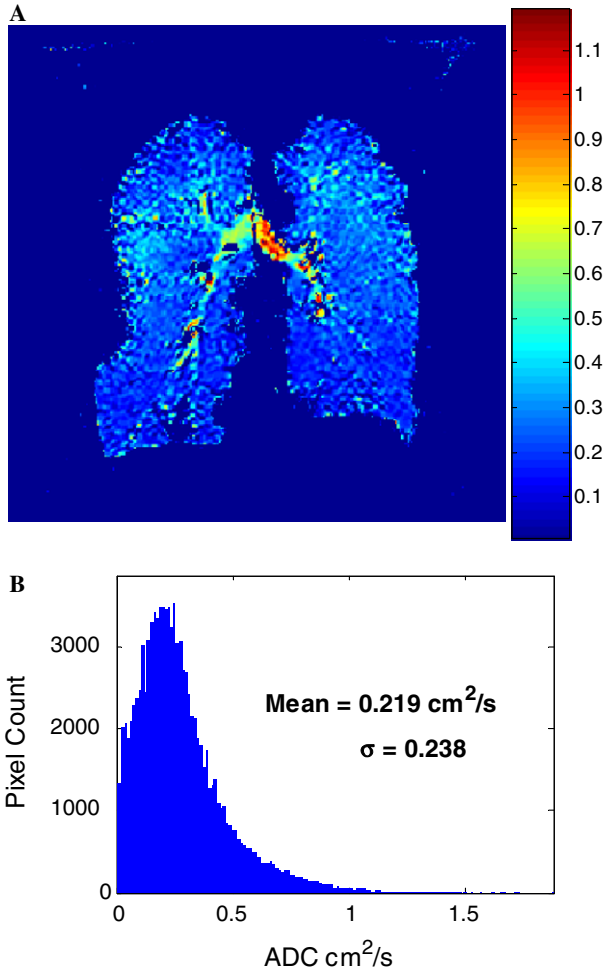

Fig. 4. ADC image (A) and histogram (B) from a 60 year old male with a 35 pack year smoking history. The units for the color bar are cm^2/s. A ventilation defect (white arrow) is apparent on the left side of the ADC image in (A).

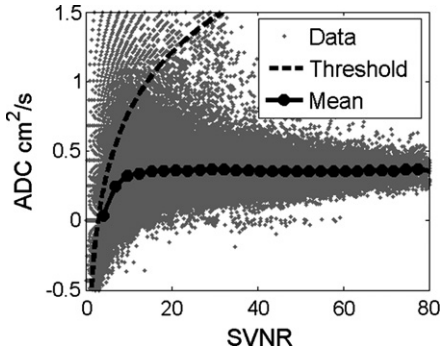

Fig. 5. ADC values measured in a human subject (gray) are shown with the threshold line indicated (dotted line). The mean ADC is calculated for points to the right of the curve within discrete SVNR bins (data points on solid line).

mean ADC is largely independent of SNR for SNR > 15 for the range of ADC values observed in human lung attesting to the sensitivity of this measure to detect early changes in lung microstructure [13,14,21]. In volunteer

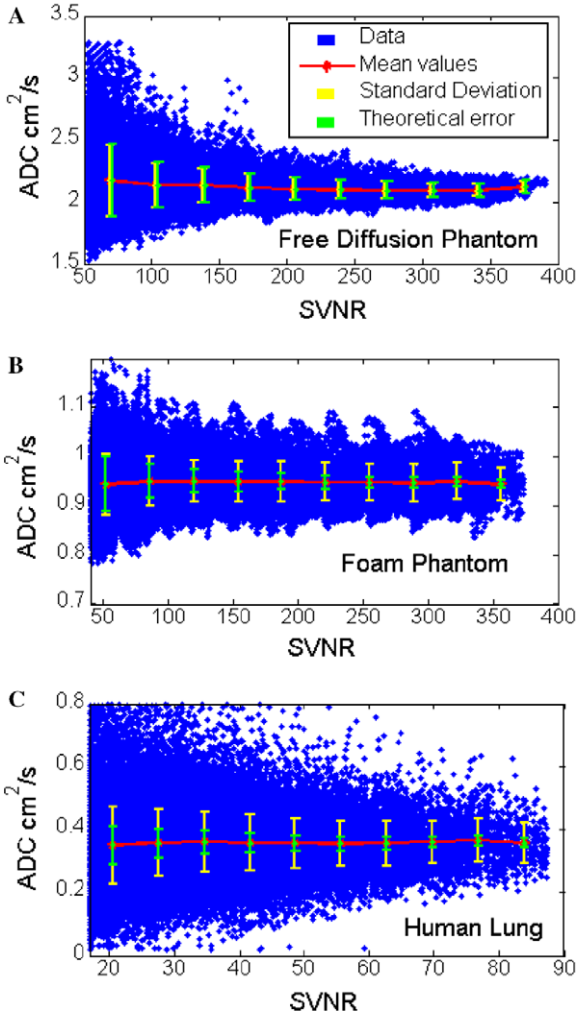

Fig. 6. ADC vs. SVNR plots for (A) the free diffusion phantom, (B) the foam phantom, and (C) human lung. The theoretical standard deviation is in agreement with the measured standard deviation for the free diffusion phantom whereas it underestimates the standard deviation in the foam phantom and human lung.

and patient studies the mean ADC values were found to be consistent with this cutoff, decreasing rapidly for SNR values near or below 10. This underestimation of the mean ADC due to values lower than this SNR can be eliminated by imposing a threshold on the unweighted image only. Although this method includes points with very low signal in the weighted image, the source of low signal in these voxels may be attributed to high diffusion or high noise. Since these two effects are indistinguishable it may be acceptable to include these points for analysis based on their high unweighted signal alone.

The dependence of σ_{ADC} on SNR in the simulation and in the free diffusion phantom was shown to obey Eq. (6) for all but the very lowest SNR values, implying the variation of the ADC measurements is purely stochastic as would be expected when there is no underlying structure to restrict diffusion. The deviations between measurement and theory for extremely low SNR in the free diffusion case are likely due to averaging over a finite bin width where the SNR

dependence is changing rapidly. In contrast, the SNR dependence over the entire range of SNR values in the foam phantom and in human lung was not fully accounted for by stochastic considerations. The remaining variation is therefore likely due to structure or, in the case of the human subject, structure and physiologic noise. The near constant value of the σ_{ADC} expected for the homogeneous foam phantom, in particular, suggests that the stochastic dependence may be removed resulting in a 'corrected' measure of standard deviation that may be a stronger metric of structural heterogeneity.

This work underscores the importance of SNR considerations in the interpretation of ADC measurements in the lungs using HP gases. Given that there is often regional overlap between sites of airway obstruction and microstructural changes associated with disease, the SNR in critical regions may be impaired by poor ventilation which can affect the accuracy of both the mean and standard deviation of the measured ADC. Moreover, the impact of thresholding on these regions is to drive down ADC values, potentially underestimating the severity of disease. In such cases, thresholding on the unweighted image only may be preferable.

Recent work has advocated multi-exponential models and diffusion tensor measurements for regional evaluation of lung structure [4,5,22,23]. These models will require thresholding that will induce similar SNR-dependence to that presented in this work for the mono-exponential model. Moreover, the mono-exponential model has been shown to capture key features of lung disease at the alveolar level and is technically less demanding for the acquisition of regional information about lung structure within the constraints of a short breath-hold. Additionally, the mean ADC from the mono-exponential model remains the most validated measure for evaluation of emphysema [4,8,11,13]. However, σ_{ADC} is an inconsistent measure of structural heterogeneity in these studies most likely due to the SNR dependence of this measure demonstrated in the present work. Consequently, there is an important need for understanding the underlying sensitivity of mean ADC and σ_{ADC} to image SNR and to what extent these measures represent stochastic vs. structural features of disease. Although the use of foam phantoms to simulate structural variation is certainly not a perfect model of the lungs, these phantoms are useful tools to help separate stochastic from structural features of disease that can guide interpretation of lung data. Moreover, similar theoretical development can help guide how to best apply more complicated multi-exponential models in future studies, and the present work provides a benchmark for the relative performance and sensitivity of these models to noise processes.

In summary, the SNR dependence of ADC measures as applied to diffusion-weighted imaging of the lung was evaluated in simulations and phantom studies. The expected error in mean ADC due to stochastic fluctuations was predicted to be less than 0.2% for mean ADC measurements below 0.6 cm^2/s and for SNR > 15. σ_{ADC} was more strongly SNR-dependent, but phantom studies suggest the stochastic component may be removed to better reflect variation in microstructure. To obtain accurate measurements of ADC, we recommend a threshold of 15 on the SVNR in the unweighted image. This is equivalent to a 15σ threshold on the *unweighted* signal only and is therefore more selective than the previously considered threshold of 2.5σ on *both* the weighted and unweighted signals. Aside from the higher threshold, the present method differs from the previous approach in that voxels are rejected based only on their unweighted signal value. In the previous approach, voxels were more likely to be rejected based on the value of their weighted signal, causing valid measures of elevated ADC to be rejected.

Appendix A

A.1. Probability density function derivation

To obtain the probability density function (PDF) of the ADC we treat the ADC as a function of two random variables, $SVNR_0$ and $SVNR_1$, with Rician PDFs. If A_0 and A_1 are the noise-free signals in the unweighted and weighted images respectively the PDFs for $SVNR_0$ and $SVNR_1$ can be expressed as,

$$P_{SVNR_0}(SVNR_0) = \frac{SVNR_0}{\sigma} \cdot e^{-\frac{1}{2}(SVNR_0^2+\frac{A_0^2}{\sigma^2})} \cdot I_0\left(\frac{SVNR_0 \cdot A_0}{\sigma}\right), \quad (A1)$$

$$P_{SVNR_1}(SVNR_1) = \frac{SVNR_1}{\sigma} \cdot e^{-\frac{1}{2}(SVNR_1^2+\frac{A_1^2}{\sigma^2})} \cdot I_0\left(\frac{SVNR_1 \cdot A_1}{\sigma}\right), \quad (A2)$$

where I_0 is the zeroth order Bessel function of the first kind and σ is the standard deviation of the noise in each of the I and Q channels. For clarity the derivation is done in two steps. First we define two new random variables RV_1 and RV_2 in Eqs. (4a–c) and obtain their PDFs. If Y is a random variable depending on another random variable, X, with known PDF, $P_x(x)$, then the PDF of Y, $P_y(y)$, can be obtained via [24],

$$Y = f(X) \quad (A3)$$

$$P_y(y) = \frac{P_x(x)}{g'(x)}, \quad (A4)$$

where $g'(x)$ denotes the derivative of g with respect to x. Using the rule given by Eqs. (A3, A4) the PDFs for RV_1 and RV_2 are,

$$P_{RV_1}(RV_1) = b \cdot e^{RV_1 \cdot b} \cdot P_{SVNR_0}(SVNR_0) \cdot (e^{RV_1 \cdot b}) \quad (A5)$$

$$P_{RV_2}(RV_2) = b \cdot e^{-RV_2 \cdot b} \cdot P_{SVNR_1}(SVNR_1) \cdot (e^{-RV_2 \cdot b}). \quad (A6)$$

If a random variable, Z, can be expressed as the sum of two random variables, X and Y, with known PDFs, $P_x(x)$ and $P_y(y)$, the PDF of Z, $P_z(z)$, can be written as [24],

$$P_z(z) = P_x(x) * P_y(y). \tag{A7}$$

Applying Eq. (A7) to Eq. (4a) we obtain the result given by Eq. (5),

$$P_{\mathrm{ADC}}(\mathrm{ADC}) = P_{\mathrm{RV}_1}(\mathrm{RV}_1) * P_{\mathrm{RV}_2}(\mathrm{RV}_2). \tag{A8}$$

A.2. Standard deviation derivation

To derive the standard deviation of the ADC, σ_{ADC}, we start with Eq. (1) from Section 2 and again assume the noise in the unweighted, σ_0, and weighted, σ_1, images is uncorrelated and that the b-value is known with negligible error from the gradient waveforms. Then,

$$\sigma^2_{\mathrm{ADC}} = \left(\frac{\partial \mathrm{ADC}}{\partial \mathrm{S}_0}\right)^2 \sigma^2 + \left(\frac{\partial \mathrm{ADC}}{\partial \mathrm{S}_1}\right)^2 \sigma^2, \tag{A9}$$

where S_0 and S_1 are the unweighted and weighted signal respectively.

Performing the differentiation of Eq. (1) and assuming the same noise magnitude, $\sigma_1 = \sigma_2 = \sigma$, one obtains:

$$\sigma^2_{\mathrm{ADC}} = \frac{\sigma^2}{b}\left(\frac{1}{\mathrm{S}_0^2} + \frac{1}{\mathrm{S}_1^2}\right). \tag{A10}$$

By substituting the expression for S_1 derived from algebraic rearrangement of Eq. (1), one obtains:

$$\sigma^2_{\mathrm{ADC}} = \frac{\sigma^2}{b}\left(\frac{1}{\mathrm{S}_0^2} + \frac{1}{\mathrm{S}_0^2}\mathrm{e}^{2\cdot b\cdot \mathrm{ADC}}\right). \tag{A11}$$

Now, by substitution of our definition of the signal-value-to-noise ratio of the unweighted image, SVNR_0, and taking the square root, we obtain the result given by Eq. (6):

$$\sigma_{\mathrm{ADC}} = \frac{1}{b}\cdot\frac{1}{\mathrm{SVNR}_0}\cdot\sqrt{1+\mathrm{e}^{2\cdot b\cdot \mathrm{ADC}}}. \tag{A12}$$

References

[1] E.O. Stejskal, J.E. Tanner, Spin diffusion measurements: spin echoes in the presence of a time-dependent field gradient, J. Chem. Phys. 42 (1965) 288–292.

[2] D. Le Bihan, J.F. Mangin, C. Poupon, C.A. Clark, S. Pappata, N. Molko, H. Chabriat, Diffusion tensor imaging: concepts and applications, J. Magn. Reson. Imaging 13 (4) (2001) 534–546.

[3] M. Salerno, J. Brookeman, E.E deLange, J. Knight-Scott, J.P. Mugler, Demonstration of an alveolar-size gradient in the healthy human lung: a study of the reproducibility of hyperpolarized ^{3}He diffusion MRI, in: Proceedings of the 8th Annual Meeting of ISMRM, Denver, CO, USA, 2000, p. 2195.

[4] A.E. Morbach, K.K. Gast, J. Schmiedeskamp, A. Dahmen, A. Herweling, C.P. Heussel, H.U. Kauczor, W.G. Schreiber, Diffusion-weighted MRI of the lung with hyperpolarized helium-3: a study of reproducibility, J. Magn. Reson. Imaging 21 (2005) 765–774.

[5] D.A. Yablonskiy, A.L. Sukstanskii, J.C. Leawoods, D.S. Gierada, G.L. Bretthorst, S.S. Lefrak, J.D. Cooper, M.S. Conradi, Quantitative in vivo assessment of lung microstructure at the alveolar level with hyperpolarized ^{3}He diffusion MRI, PNAS 99 (2002) 3111–3116.

[6] X.J. Chen, L.W. Hedlund, H.E. Möller, M.S. Chawla, R.R. Maronpot, G.A. Johnson, Detection of emphysema in rat lungs by using magnetic resonance measurements of ^{3}He diffusion, PNAS 97 (2000) 11478–11481.

[7] M. Salerno, J. Mugler, E.E. deLange, J. Brookeman, T. Altes, Detection of early smoking related lung diseases with diffusion-weighted hyperpolarized helium-3 MR lung imaging, in: RSNA 89th Scientific Assembly and Annual Meeting. Chicago, IL, USA, 2003, p. 526.

[8] M. Salerno, E.E. de Lange, T.A. Altes, J.D. Truwit, J.R. Brookeman, J.P. Mugler, Emphysema: hyperpolarized helium-3 diffusion MR imaging of the lungs compared with spirometric indexes—initial experience, Radiology 222 (2002) 252–260.

[9] M.D. Hayhurst, W. MacNee, D.C. Flenley, D. Wright, A. McLean, D. Lamb, A.J.A. Wightman, J. Best, Diagnosis of pulmonary emphysema by computerized tomography, Lancet 2 (1984) 320–322.

[10] X.J. Chen, H.E. Möller, M.S. Chawla, G.P. Cofer, B. Driehuys, L.W. Hedlund, G.A. Johnson, Spatially resolved measurements of hyperpolarized gas properties in the lung in vivo. Part I: diffusion coefficient, Magn. Reson. Med. 42 (1999) 721–728.

[11] B. Saam, D.A. Yablonskiy, V.D. Kodibagkar, J.C. Leawoods, D.S. Gierada, J.D. Cooper, S.S. Lefrak, M.S. Conradi, MR imaging of diffusion of ^{3}He gas in healthy and diseased lungs, Magn. Reson. Med. 44 (2000) 174–179.

[12] D.S. Gierada, Radiologic assessment of emphysema for lung volume reduction surgery, Semin. Thorac. Cardiovasc. Surg. 14 (4) (2002) 381–390.

[13] A.J. Swift, J.M. Wild, S. Fichele, N. Woodhouse, S. Fleming, J. Waterhouse, R.A. Lawson, M.N.J. Paley, E.J.R. Van Beek, Emphysematous changes and normal variation in smokers and COPD patients using diffusion 3He MRI, Eur. J. Radiol. 54 (2005) 352–358.

[14] S.B. Fain, S.R. Panth, M.D. Evans, A.L. Wentland, J.H. Holmes, F.R. Korosec, H. Fountaine, T.M. Grist, ^{3}He MRI detects early emphysematous changes in asymptomatic smokers, Radiology 239 (2006) 875–883.

[15] M. Salerno, J.R. Brookeman, E.E. deLange, J.P. Mugler, The effect of SNR on helium-3 ADC values in the lung, in: Proceedings of the 11th Annual Meeting of ISMRM, Toronto, Canada, 2003, p.1386.

[16] R.M. Henkelman, Measurement of signal intensities in the presence of noise in MR images, Med. Phys. 12 (1985) 232–233.

[17] H. Gudbjartsson, S. Patz, The Rician distribution of noisy MRI data, Magn. Reson. Med. 34 (1995) 910–914.

[18] M. Salerno, Hyperpolarized ^{3}He diffusion MRI for characterizing the human lung, PhD Thesis, University of Virginia, 2003.

[19] A.B. Baranga, S. Appelt, M.V. Romalis, C.J. Erickson, A.R. Young, G.D. Cates, W. Happer, Polarization of ^{3}He by spin exchange with optically pumped Rb and K vapors, Phys. Rev. Lett. 80 (1998) 2801–2804.

[20] A. Sukstankii, Y.V. Chang, G.L. Bretthorst, M.S. Conradi, D.A. Yablonskiy, How to optimize b-values for *in vivo* lung morphometry with ^{3}He diffusion MR, in: Proceedings of the 14th Annual Meeting of ISMRM, Seatle, USA, 2006, p.1316.

[21] S.B. Fain, T.A. Altes, S.R. Panth, M.D. Evans, B. Waters, J.P. Mugler III, F.R. Korosec, T.M. Grist, M. Silverman, M. Salerno, J. Owers-Bradley, Detection of age-dependent changes in healthy adult lungs with diffusion-weighted ^{3}He MRI, Acad. Radiol. 12 (2005) 1385–1393.

[22] D.D. Shanbhag, T.A. Altes, G.W. Miller, J.F. Mata, J. Knight-Scott, q-Space analysis of lung morphometry in vivo with hyperpolarized 3He spectroscopy, J. Magn. Reson. Imaging 24 (1) (2006) 84–94.

[23] W.G. Schreiber, A.E. Morbach, T. Stavngaard, K.K. Gast, A. Herweling, L.V. Søgaard, M. Windirsch, J. Schmiedeskamp, C.P. Heussel, H. Kauczor, Assessment of lung microstructure with magnetic resonance imaging of hyperpolarized helium-3, Respir. Physiol. Neurobiol. 148 (2005) 23–42.

[24] A. Papoulis, Probability, Random Variables, and Stochastic Processes, third ed., McGraw-Hill Book Company, Boston, 1991.